Co_2MnX (X=Si, Ge, Sn) Heusler compounds: An *ab initio* study of their structural, electronic, and magnetic properties at zero and elevated pressure

S. Picozzi and A. Continenza
Istituto Nazionale di Fisica della Materia (INFM), Dipartimento di Fisica, Università degli Studi di L'Aquila, 67010 Coppito (L'Aquila), Italy

A. J. Freeman
Department of Physics and Astronomy and Materials Research Center, Northwestern University, Evanston, Ilinois 60208
(Received 16 April 2002; revised manuscript received 12 July 2002; published 17 September 2002)

The structural, electronic, and magnetic properties of Co_2MnX (X=Si, Ge, Sn) Heusler compounds have been determined by means of all-electron full-potential linearized augmented plane wave (FLAPW) calculations. We focus on the effects on the electronic and magnetic properties induced by: (i) substitution of the X atom, (ii) applied pressure, and (iii) the use of the local spin density approximation (LSDA) vs the generalized gradient approximation (GGA) in density functional theory. A comparison between LSDA and GGA for the exchange-correlation functional shows that GGA is essential for an accurate description of the equilibrium volumes and of the electronic and magnetic properties of these systems. We find that both the energy gap and the spin gap increase as the X atomic number decreases. As a result of the semiconducting (metallic) character found in the minority (majority) spin band structure, the Si and Ge based alloys are predicted to be half-metallic. In contrast, Co_2MnSn is found to be a ''nearly half-metallic'' compound, since the minority valence band maximum crosses the Fermi level. The calculated total magnetization of 5 μ_B is in excellent agreement with recent experiments. By including a fully self-consistent treatment of spin-orbit coupling, the GGA calculated orbital moments are shown to be very small (about 0.008 μ_B for Mn and about 0.02 μ_B for Co), showing that the quenching of the orbital magnetic moment is nearly complete. The calculated hyperfine fields, both at zero and elevated pressure, are compared with available experimental data, and show general agreement, except for Mn. Finally, the calculated Mn $2p$ exchange splittings, found to be in good agreement with experiment, are proportional to the Mn magnetic moments, suggesting a localized nature of ferromagnetism in these Heusler compounds.

DOI: 10.1103/PhysRevB.66.094421 PACS number(s): 75.50.Cc, 71.20.Be

I. INTRODUCTION

The crucial issue of spin-injection from a ferromagnet into a semiconductor is attracting growing interest,[1,2] due to its importance for the realization and performance of practical devices in the emerging field of spintronics.[3,4] In particular, most magnetoelectronic devices rely on an imbalance in the number of majority and minority spin carriers, with the ideal material exhibiting a complete (100%) spin-polarization at the Fermi surface [i.e., a half-metallic ferromagnet (HMF)].[5] Within this framework, the Heusler intermetallic alloys, some of which have been predicted from first-principles calculations to be half-metallic,[5–7] represent a promising set of compounds.[8]

Mn is a special element in this class of materials, since almost all the known HMF (except for CrO_2 and a few others) are Mn based compounds. Cobalt, when used as the first atom in Co_2MnX-like compounds (where X is a type III or type IV element), was found[9] to give tremendous stability to the ferromagnetic alignment, resulting in measured Curie temperatures of 985 K, 905 K, and 829 K in Co_2MnSi, Co_2MnGe, and Co_2MnSn (see Refs. 9, 10, and references therein), respectively.

Motivated by these issues, there has recently been renewed experimental interest in the Co_2MnX (X=Si, Ge) Heusler alloys. Raphael *et al.*[11] have successfully grown Co_2MnSi and Co_2MnGe films and found, by performing SQUID magnetometry and point contact Andreev reflection measurements, a saturation magnetization of $5.01 \leqslant \mu \leqslant 5.15$ μ_B and a spin-polarization of about 50%–60%, suggesting either that the films are not HMF or that the full spin polarization is limited by antisite defects. Within this same research field, Ambrose *et al.*[12] deposited Co_2MnGe films on a GaAs substrate by molecular beam epitaxy; their measurements revealed the perfect crystallinity of the Heusler films up to a 350 Å film thickness and a large magnetization along with a small magnetic anisotropy.

From the theoretical point of view, pioneering first-principles calculations were performed for bulk Co_2MnSn,[9,13] Co_2MnGe,[13] and, more recently, for Co_2MnSi (Ref. 13,14) at the experimental equilibrium lattice constants using the local spin density approximation (LSDA).[15] It is well-known,[16] however, that this approximation systematically predicts underestimated lattice constants compared to experiments for $3d$ elements and, as a by-product, smaller magnetic moments. For example, it was shown[17] that the LSDA error in the equilibrium volume of Mn pnictides (MnAs and MnSb)—as large as 20%—can be completely recovered using the generalized gradient approximation (GGA).[18]

In this work, we present a comprehensive investigation of the equilibrium structural, electronic and magnetic properties

TABLE I. Equilibrium structural properties within LSDA, GGA and experiment (where available). The lattice constant a and the bulk modulus B are in a.u. and in GPa, respectively.

	Co_2MnSi			Co_2MnGe			Co_2MnSn		
	LSDA	GGA	expt	LSDA	GGA	expt	LSDA	GGA	expt
a	10.42	10.65	10.68[a]	10.61	10.84	10.85[a]	11.04	11.27	11.34[a], 11.30[b]
B	264	226	···	241	188	···	270	187	···

[a]Reference 25.
[b]Reference 26.

of Co_2MnX (X=Si, Ge, Sn), focusing on the effect of the group IV atom, of the applied pressure and on the differences between LSDA and GGA treatments. In Sec. II, we report some details about the crystal structure and some computational technicalities; we concentrate in Sec. III A on the equilibrium lattice constant and bulk modulus; in Sec. III B, we discuss the electronic properties in terms of band structures and density of states; in Sec. III C we focus on the Mn $2p$ exchange splittings, hyperfine fields,[19] and magnetic moments; in Sec. IV, we analyze the dependence on pressure of the relevant electronic and magnetic properties; finally, we draw conclusions in Sec. V.

II. THE HEUSLER CRYSTAL STRUCTURE AND COMPUTATIONAL DETAILS

Many of the Heusler alloys have a cubic $L2_1$ structure (space group $Fm3m$), which can be thought of as a simple cubic lattice for Co atoms, with the Mn and X atoms arranged at alternate body centered positions.

The calculations were performed within the framework of density-functional theory, using the highly accurate all-electron full-potential linearized augmented plane wave (FLAPW) (Ref. 20) method. The core levels are treated fully relativistically, whereas the valence electrons are calculated semi-relativistically, i.e., without spin-orbit coupling. In order to calculate orbital magnetic moments in the equilibrium structures, we also performed calculations including a fully self-consistent treatment with the spin–orbit interaction included. The exchange–correlation potential is treated within (i) the local spin density approximation (LSDA) using the von Barth–Hedin parametrization[15] and (ii) the generalized gradient approximation (GGA) according to the Perdew–Becke–Ehrenzhof parametrization.[18] It was pointed out[21,22] and found[23] that LSDA has a tendency to reduce the charge asphericity, while GGA, including nonlocal contributions, can enhance such effects, also resulting in a more accurate description of the energy bands; it is therefore particularly important to use GGA in these compounds, employing a full-potential band structure method.

The muffin tin spheres were chosen as $R_{MT}^{Co}=R_{MT}^{Mn}=R_{MT}^{Ge}=2.1$ a.u., $R_{MT}^{Si}=2.0$ a.u., and $R_{MT}^{Sn}=2.3$ a.u., and the expansion in spherical harmonics in these regions was performed up to $l\leqslant 8$; in the interstitial part, a cutoff for the wave functions $k_{max}=3.8$ a.u.$^{-1}$ was used. The Brillouin zone sampling was performed according to the Monkhorst–Pack scheme,[24] using 60 **k** points [shell (10,10,10)] in the irreducible wedge of the zone.

III. ZERO PRESSURE PROPERTIES

A. Structural properties

The equilibrium lattice constant and bulk modulus were calculated using both LSDA and GGA; the results are compared with available experimental data[25,26] in Table I. Total energies as a function of pressure were interpolated according to the semiempirical Murnaghan equation of state,[27]

$$P=\frac{B_0}{B_0'}\left[\left(\frac{a_{eq}}{a}\right)^{3B_0'}-1\right], \tag{1}$$

where B_0 is the bulk modulus, B_0' is its derivative with respect to pressure, a_{eq} the equilibrium lattice constant, and a the lattice constant at pressure P.

A comparison between the equilibrium lattice constants predicted using LSDA and GGA for the exchange and correlation functional shows that GGA is essential to accurately reproduce the equilibrium structural properties of these Heusler alloys. In fact, LSDA underestimates the equilibrium volume by about 7% with respect to experiment, whereas the GGA error is at most 1%, following the general tendency found for the $3d$ elements; due to its functional form, GGA gives larger lattice constants and this results in a better agreement with experiment compared to LSDA.[16] As expected, the lattice constant increases as we increase the X atomic number (by 1.8% when substituting Ge for Si and by 3.7% upon substituting Sn for Ge). As for the lattice matching with respect to standard semiconductors to be used in spintronic devices, as is well-known Co_2MnSi seems the most promising material. In fact, its lattice mismatch with GaAs and AlGaAs (used, for example, as quantum wells and side layers, respectively, in the first spin-light emitting diode[28]) is $<0.4\%$; however, this is not the only parameter that determines a successful spin-injection, which is also crucially controlled by band line-ups and transport properties across the Heusler/semiconductor interface.

We see from Table I that the GGA bulk moduli are also systematically smaller than LSDA, as already observed for the $3d$ ferromagnetic metals.[29] Since we are not aware of any experimental data, we follow an approach similar to Ref. 30: to estimate the interatomic distances as a function of pressure in Co_2MnSn, Gavriliuk *et al.*[30] used the isothermal compressibility of Ni_2MnSn, assuming Co and Ni not to differ too much. We obtain the compressibility α from the standard equation of state for solids,

$$\frac{V-V_{\mathrm{eq}}}{V_{\mathrm{eq}}} = -\alpha \cdot P + \beta \cdot P^2. \quad (2)$$

In our case, the GGA and LSDA predicted values are $\alpha^{\mathrm{GGA}} = 5.9 \cdot 10^{-3}$ GPa^{-1} and $\alpha^{\mathrm{LSDA}} = 4.1 \cdot 10^{-3}$ GPa^{-1}, respectively, to be compared with the experimental value for Ni_2MnSn of $7.7 \cdot 10^{-3}$ GPa^{-1}. It therefore seems that the GGA results are in better agreement with experiment,[30] and so results in an overall more accurate description of the structural properties of these Heusler compounds.

B. Electronic properties

We show in Fig. 1 the GGA spin-polarized band structure[31] for the Heusler compounds at equilibrium (to our knowledge, GGA band structures have not been reported previously). The lowest valence band (from -12 eV to -9 eV in both the majority and minority spin states) is almost entirely due to X s electrons and is separated with respect to the other hybridized bands, being basically unaffected by the Mn and Co exchange interaction. The upper dispersed bands are due to the strong hybridization of Mn d and Co d electrons, including a contribution from X p states in the occupied valence states. In particular, at Γ there is a series of twofold degenerate states (e_g) derived entirely from Mn and Co d states and threefold degenerate states (t_{2g}) that allow hybridization of Mn and Co d states with the X p states.

The majority spin band structure is strongly metallic, while the minority spin band structure shows a semiconducting gap around the Fermi level, E_F, except in Co_2MnSn, where the minority "valence band maximum" (VBM) is just slightly above E_F, leading to a "nearly half-metallic" behavior.[32] On the other hand, half-metallicity is marked in Co_2 MnSi and Co_2MnGe; the GGA calculated indirect $\Gamma - X$ band gap for minority carriers is $E_{\mathrm{gap}}(Co_2MnSi) = 0.81$ eV and $E_{\mathrm{gap}}(Co_2$ MnGe$) = 0.54$ eV, respectively, while the Fermi level lies 0.33 eV and 0.03 eV above the minority spin VBM, respectively.[33] This last and very important quantity is often referred to as the "spin-gap," i.e., the minimum energy required to flip a minority spin electron from the VBM to the majority spin Fermi level.[34]

In Fig. 2 we show the positions of the minority VBM (at Γ) and CBM (at X) with respect to E_F and the resulting band gaps, as a function of the (i) exchange and correlation functional, (ii) X atom, and (iii) lattice constant. Note that within the same exchange and correlation functional and for a given compound, volume compression leads to a slight increase of the minority band gap, whereas E_F is progressively shifted from the valence band into the band gap [see Figs. 2(b), 2(c), 2(e), 2(f)]. Similar features have been found for other Heusler compounds; in particular, it was shown in Ref. 7 that PdMnSb is not a half-ferromagnet at ambient pressure, but becomes one at higher hydrostatic pressures, due to increased hybridization between Mn $3d$ and Pd $4d$ states. Moreover, at fixed lattice constant and atomic constituents, GGA predicts a slightly larger band gap compared to LSDA; the conduction bands are shifted upwards, while E_F is more or less fixed with respect to the valence band maximum.

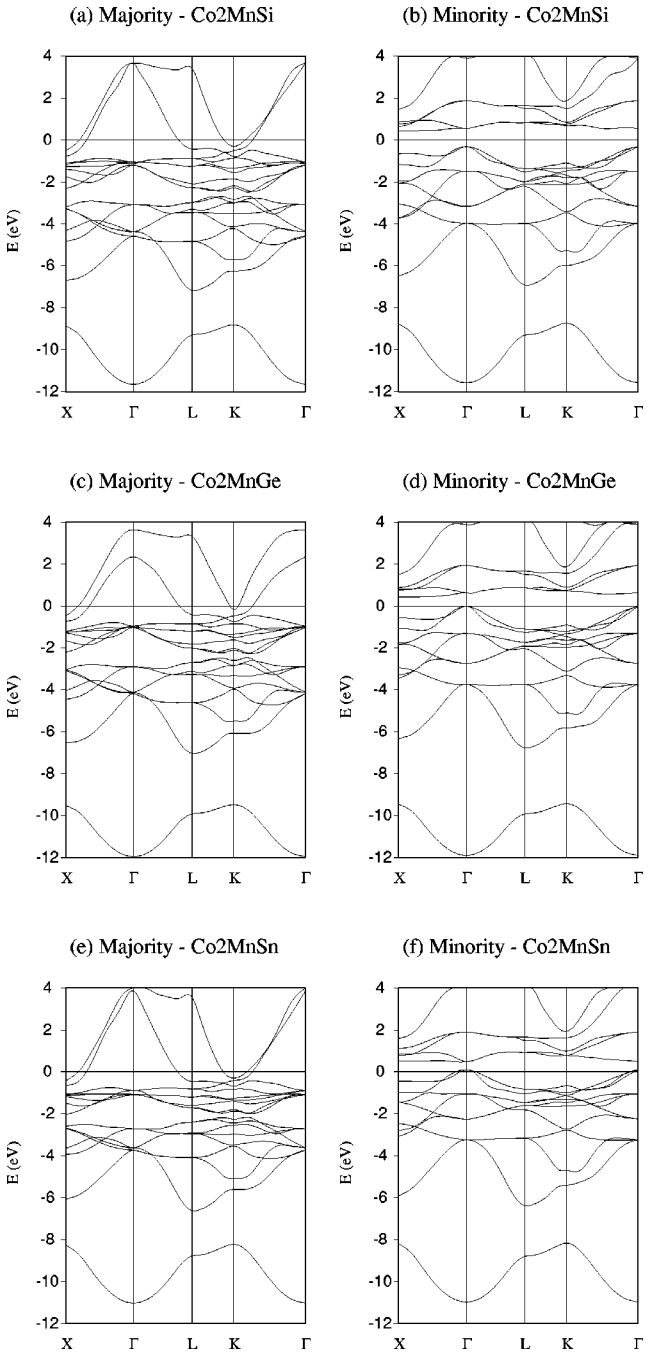

FIG. 1. Majority spin (left column) and minority spin (right column) band structures for Co_2MnSi [(a),(b) panels, respectively], Co_2MnGe [(c),(d) panels, respectively], and Co_2MnSn [(e),(f) panels, respectively].

Finally, we point out that both the energy gap and spin gap increase as the X atomic number decreases. While both are excited state properties, and hence are incorrectly given in both LDA and GGA, the predicted trends are expected to be correct.

A potential candidate for spin-injection is the Co_2MnGe/GaAs junction[12] and it is therefore relevant to know whether Co_2MnGe grown on a [001] GaAs substrate will retain its half-metallic character, despite the 1.5% lattice mismatch. Our GGA calculations show that the substrate

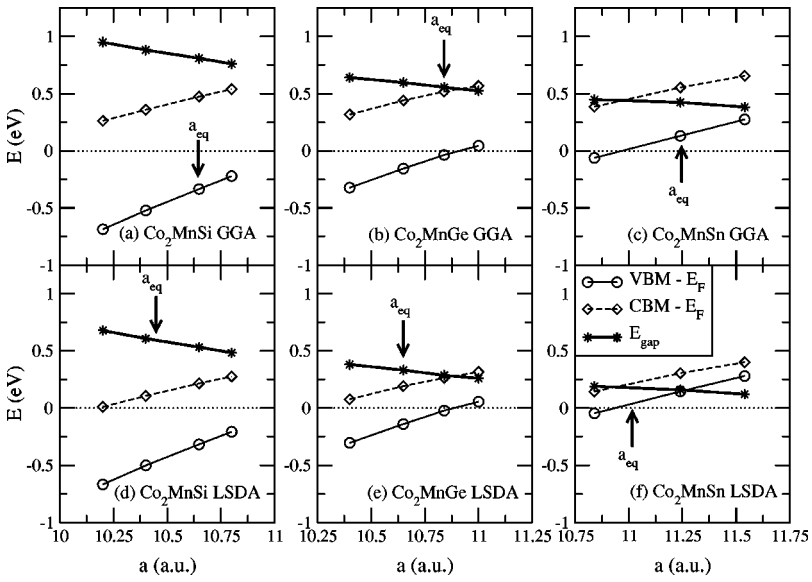

FIG. 2. Minority VBM (circles), CBM (diamonds) and band gap (stars) as a function of lattice constant for Co_2MnSi [GGA and LSDA in panels (a) and (d), respectively], Co_2MnGe [GGA and LSDA in panels (b) and (e), respectively], Co_2MnSn [GGA and LSDA in panels (c) and (f), respectively], all in eV. The Fermi level is set to zero in the energy scale.

constraint induces a tetragonal distortion on the Heusler structure, so that the lattice constant parallel to the growth direction becomes 3% larger than the in-plane parameter. In this geometry, the calculated energy- and spin-gaps are 0.47 eV and 0.09 eV, respectively, showing that the half-metallic character is kept under pseudomorphic growth conditions.

The highest occupied minority spin state at Γ is a triply degenerate p–d hybridized t_{2g} state, so that the decreasing binding energy of this state with respect to E_F along the Si $\rightarrow$ Ge $\rightarrow$ Sn series can therefore be traced back to two combined effects: (i) p–d hybridization, which obviously depends on the X p states and (ii) their different lattice constants. In this respect, as already pointed out, we note from Fig. 2 that at fixed lattice constant and with the same exchange and correlation functional, the substitution of the X atom alters slightly both the position of E_F and the band gap.

Further insights regarding the hybridization, which comes into play in the bonds characterizing these compounds, can be gained from the GGA calculated total and atomic-projected density of states (DOS) shown in Fig. 3. In the majority spin component, Mn 3d states are occupied and hybridized with Co 3d electrons; on the other hand, in the minority spin part, local and mostly non-hybridized Mn 3d states are found at about 1.5 eV above E_F. The different X atoms provide s–p states to be hybridized with d electrons and determine the degree of occupation of p-d orbitals. In particular, we note that features of the Mn projected density of states (PDOS) [shown in Fig. 3(c)] can be traced back to the e_g–t_{2g} splittings of Mn 3d levels in a cubic crystal field: the majority (minority) spin states, show two well-separated peaks at -3 and -1 eV (-1.5 and 1.5 eV). On the other hand, the e_g–t_{2g} splitting is not so evident in the Co majority PDOS, which does not reveal any prominent features. However, a deeper investigation shows that if we substitute all the Ge sites with Mn, ending up with an ideal CoMn intermetallic ordered alloy, we recover the two main peaks in the Co majority PDOS characteristic of the e_g–t_{2g} cubic splitting. Therefore, states in the ''valley'' between the two main peaks are induced by the strong Ge p–Co d hybridization (as suggested by the corresponding features in the Ge PDOS at the same energies).

Although the overall features are similar in all three compounds, it is evident that there are some differences in the DOS of these Heusler alloys due to both the presence of different X atoms and different volumes. In particular, let us focus on the feature in the minority spin total DOS (at around -1 eV) due to the Mn and Co d states hybridized with X p states, whose tail determines the character of the minority spin VBM. This peak gains an increasing binding energy along the Sn$\rightarrow$Ge$\rightarrow$Si series. As previously stated in the discussion relative to the band structure, the different group IV element is responsible for the loss of the half-metallicity in the Sn compound. The Mn PDOS in the Si-,Ge-, and Sn-based Heusler alloys is very similar and is characterized by the d exchange splitting (i.e., the difference between the main peaks of majority occupied and minority unoccupied states), ΔE_x, of about 2.8 eV.

C. Magnetic properties

The calculated LSDA, GGA, and experimental magnetic moments for the compounds and for the single constituents are reported in Table II and compared with available experiments.[11,12,25,35,26] The Mn atom carries the largest moment (around 3 μ_B), while Co has a positive moment of about 1 μ_B. The X atom is slightly antiferromagnetically spin-polarized with respect to Mn and Co. The total moment in all three compounds is 5 μ_B, which is in good agreement with experimental values;[11,12] we point out that the integer value of the total magnetic moment is an indication of the half-metallic character (complete, as in Si and Ge compounds, or ''nearly'' complete, as in the Sn compound). The Mn magnetic moment appears to be slightly underestimated with respect to experiment for Co_2MnSn.[36]

As for the trends with the X atomic number, we note that the Mn magnetic moment increases slightly along the Si $\rightarrow$Ge$\rightarrow$Sn series; this can be ascribed to the increasingly

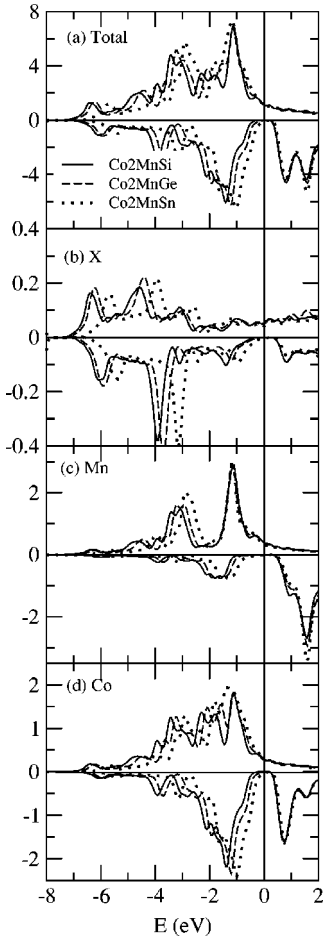

FIG. 3. Density of states of Co_2MnSi (solid), Co_2MnGe (dashed), and Co_2MnSn (dotted) compounds: (a) total and projected on (b) X, (c) Mn, and (d) Co atoms.

larger lattice constant of the Mn sublattice, which results[16] in a smaller d–d overlap and a consequently larger exchange interaction. On the other hand, the Co magnetic moment is reduced as the anion atomic number increases, keeping the global magnetic moment very close to 5 μ_B. To describe the magnetic behavior of these Heusler alloys, we observe that at least three different mechanisms should be taken into account: (i) the superexchange mechanism through the sp electrons of the group IV atom; (ii) the s–d_{Mn} interaction between the s conduction electrons and the localized d_{Mn} electrons via a Ruderman–Kittel-Kasuya–Yoshida-type exchange, due to the large Mn–Mn distance; and (iii) the d_{Mn}–d_{Co} interaction, resulting in a common d band with rather delocalized d electrons. The mechanisms leading to the actual Co magnetic moment are therefore quite complicated.

Since it was suggested[13] that Co may have an unquenched orbital magnetic moment, we calculated fully self-consistently the spin–orbit coupling and evaluated the Mn and Co orbital polarizations. In all three compounds, the GGA calculated orbital moments are very close to zero (about 0.008 μ_B) for Mn and about 0.02 μ_B for Co, showing that the quenching of the orbital magnetic moment, due to the cubic symmetry, is nearly complete.

As a further check on our predictions, we investigate the magnetic hyperfine fields, that were also determined experimentally for these same compounds using Mössbauer spectroscopy[26] and/or nuclear magnetic resonance.[10] The hyperfine field[19] consists of several contributions: a dipolar term, an orbital term, and the leading term due to the Fermi contact interaction determined by the spin density at the nucleus,[19]

$$H_{\mathrm{hf}} = \tfrac{8}{3}\pi\mu_B^2[\rho_\uparrow(0) - \rho_\downarrow(0)], \tag{3}$$

in the scalar relativistic limit.[37] (In the fully-relativistic case, the spin density at the nucleus can be replaced by its average over the Thomson radius, $r_T = Ze^2/mc^2$.) Equation (3) takes into account the dominant exchange polarization of the core electrons, emphasizing the importance of using an all-electron method.[20]

Our calculated H_{hf} values given in Table III are broken down into total, core and valence contributions for the different atoms in the compounds at their equilibrium lattice constants; experimental values[10,26] are also given for comparison. The sign of the hyperfine field for both Mn and Co is negative, in agreement with nuclear magnetic resonance (NMR) experiments. The separation of the negative core and positive valence contributions to the Fermi contact hyperfine field highlights two opposite terms: as discussed in previous theoretical work for transition metals,[19] the large and negative core contribution can be attributed to the attraction of its majority spin electrons towards the spatial region of the spin-polarized d shell. The resulting excess of minority spin elec-

TABLE II. LSDA and GGA calculated total spin moment and magnetic moments (in Bohr magnetons) within the muffin tin spheres at their respective equilibrium, compared with available experiments.

	Co_2MnSi			Co_2MnGe			Co_2MnSn		
	LSDA	GGA	expt	LSDA	GGA	expt	LSDA	GGA	expt
μ_{tot}	5.0	5.0	$5.01 \leqslant \mu \leqslant 5.15$[a]	5.0	5.0	5.11[b]	5.0	5.0	5.08 ± 0.05[c]
μ_{Mn}	2.81	2.92	· · ·	2.88	2.98	· · ·	2.98	3.09	3.6[d], 4[e]
μ_{Co}	1.07	1.06	· · ·	1.02	1.02	· · ·	0.98	0.99	0.75[d]
μ_X	−0.02	−0.04	· · ·	−0.02	−0.03	· · ·	−0.03	−0.05	· · ·

[a]Reference 11.
[b]Reference 12.
[c]Reference 25.
[d]Reference 35.
[e]Reference 26.

TABLE III. LSDA and GGA calculated total, core and valence contribution to the hyperfine field (in kG) for the constituent atoms.

	Co_2MnSi			Co_2MnGe			Co_2MnSn		
	LSDA	GGA	expt	LSDA	GGA	expt	LSDA	GGA	expt
H_{hf}^{tot}(Mn)	−253	−249	−335.9[a]	−262	−254	−339.4[a]	−260	−253	−344.1[a]
H_{hf}^{core}(Mn)	−381	−432	···	−395	−443	···	−413	−462	···
H_{hf}^{val}(Mn)	128	183	···	133	188	···	153	209	···
H_{hf}^{tot}(Co)	−70	−120	−145[a]	−77	−122	−140.2[a]	−115	−156	−156.0[a]
H_{hf}^{core}(Co)	−147	−155	···	−142	−150	···	−139	−149	···
H_{hf}^{val}(Co)	77	36	···	65	28	···	24	−7	···
H_{hf}^{tot}(X)	17	26.0	···	137	175	···	38	132	105±3[b]

[a]NMR frequencies from Ref. 10; the sign was inferred from previous works.
[b]Mössbauer spectroscopy from Ref. 26.

trons present at the nucleus, produces a consequent negative sign of the core hyperfine field.

The Mn and Co total hyperfine fields generally increase in magnitude as a function of the X atomic number, even though the variations (especially for Mn) are quite small. A more marked trend can be seen for the core contributions. As discussed previously, as the X atomic number increases, the Mn (Co) magnetic moment increases (decreases); this results in an increasing (decreasing) core polarization, due to the exchange interaction of the polarized electrons with the s orbitals of the core. As already pointed out for other magnetic systems,[19,38,39] the core hyperfine field scales very precisely with the magnetic moment within each sphere; in agreement with other systems,[38,39] we find that the average ratio $R=H_{core}^{hf}/\mu$ for both Mn and Co is about 150 kGs/μ_B and 140 kG/μ_B within GGA and LSDA approximations, respectively. As for the magnitude of the field, the net field on Mn is much larger than that on Co, as expected from the larger magnetic moment. Moreover, we find values for Mn that are significantly smaller than NMR experiments, but fully consistent with previous LSDA Korringa–Kohn–Rostoker calculations.[13] The comparison between our GGA and LSDA calculated values reveals that both the oppositely signed core and valence contributions are larger for the nonlocal than for the local parametrization of the exchange-correlation potential. However, the total hyperfine field is more or less unaltered for Mn, whereas GGA largely improves the agreement with experiment for Co. The complexity of the hyperfine results for all compounds is seen from the fact that whereas H_{hf}^{tot}(Mn) is very close in both LSDA and GGA, H_{hf}^{tot}(Co) differs - even though the Mn moments in LDA and GGA differ by 0.10–0.11 μ_B—whereas the Co moments differ by at most 0.01 μ_B.

Comparing our results with experiment, we find a quite good consistency (both in sign and magnitude) between our GGA values and a recent Mössbauer experiment for the Sn transferred hyperfine interaction in Co_2MnSn.[26] Here GGA produces a strong improvement over the LSDA values, almost recovering the experimental result. In view of the fact that the hyperfine field results from polarization of the inner X s shells, induced by interaction with the polarized conduction electrons and by the interaction with the Mn and Co $3d$ moments, the agreement obtained is surprising. The small magnetic moment of the X atom results in a negligible core contribution ($<0.5\%$) to the final hyperfine field.

IV. PRESSURE DEPENDENCE OF THE MAGNETIC PROPERTIES

In Fig. 4, we show the magnetic moments in the Mn, Co, and X muffin tin spheres as a function of applied pressure [where according to Eq. (1), ''negative'' pressures indicate an expansion with respect to the equilibrium phase]. Note that the total magnetic moment is always 5 μ_B, but the indi-

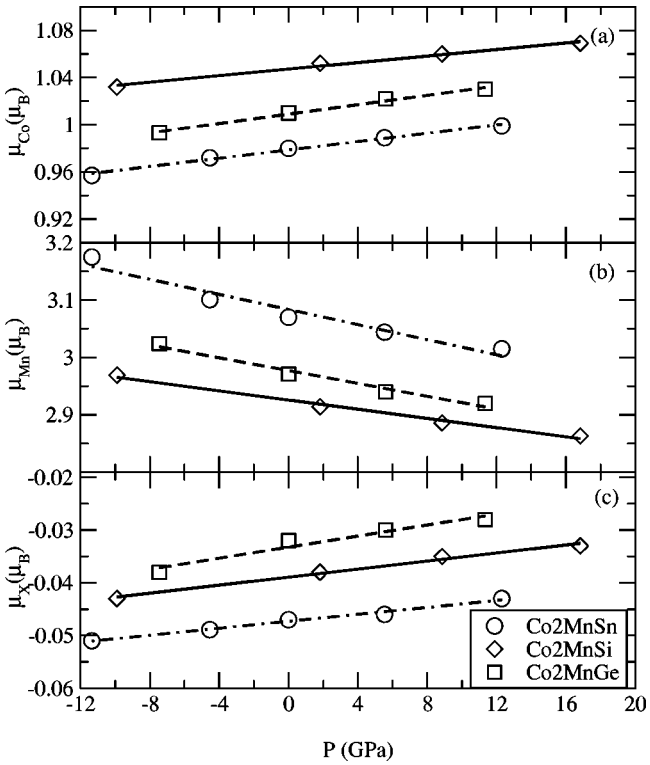

FIG. 4. Magnetic moments of Co_2MnSi (diamonds and solid line), Co_2MnGe (squares and dashed line), and Co_2MnSn (circles and dotted–dashed line) compounds in the (a) Co, (b) Mn, and (c) X muffin tin spheres vs applied pressure.

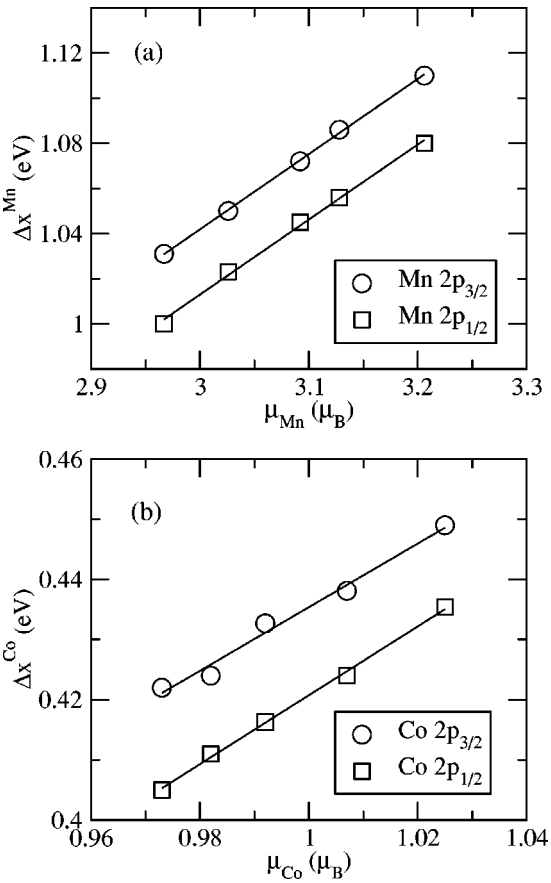

FIG. 5. Exchange splittings (in eV) of the $2p_{1/2}$ (circles) and $2p_{3/2}$ (squares) states vs magnetic moments (in Bohr magnetons) for (a) Mn and (b) Co in Co_2MnSn.

vidual moments on the atoms depend on the pressure. As expected, the Mn magnetic moments increase with decreasing pressure; again, this general behavior, found also for bulk Mn,[16] can be explained considering that as the Mn atoms are pulled apart the increased $3d$ localization leads to larger magnetic moments. On the other hand, a sort of compensating mechanism is present for Co, which shows the opposite behavior—its magnetic moment decreases as the lattice constant increases, so that the global magnetic moment is equal to 5 μ_B. A similar behavior was found in PdMnSb;[7] the induced magnetic moment on the Pd site decreases upon expansion and has to be ascribed to reduced Mn–Pd hybridization.

The Heusler intermetallic compounds have generally been considered as systems exhibiting localized magnetic moments, at variance with the general picture of itinerant d

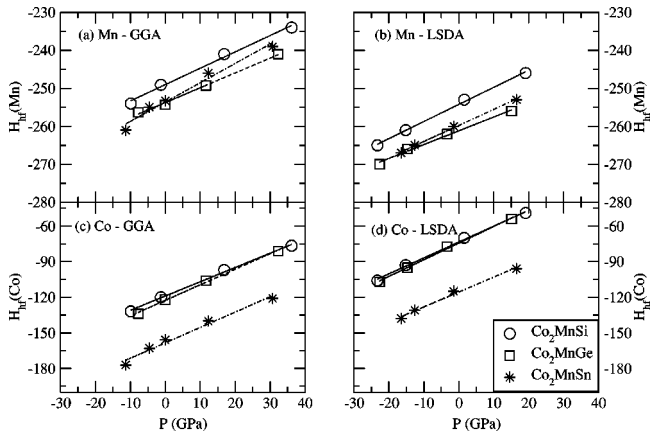

FIG. 6. Total hyperfine fields (in kG) for Mn [(a) and (b) within GGA and LSDA, respectively] and Co [(c) and (d) within GGA and LSDA, respectively] atoms for Co_2MnSi, Co_2MnGe, and Co_2MnSn vs pressure (in GPa).

electrons. It was reported from x-ray photoemission spectroscopy[36] that Mn $2p_{3/2}$ core level spectra exhibit an exchange energy splitting[40] of about 1.0–1.5 eV, whereas a separation in energy between the Mn $2p_{1/2}$ levels was not clearly evident in the spectra. It was suggested[36] that the exchange splitting gives direct evidence of the existence of well-defined local magnetic moments at the Mn site. Our fully-relativistic treatment for core electrons allows a complete study of the Mn $2p_{3/2}$ and $2p_{1/2}$ exchange splittings. In Figs. 5(a) and 5(b), we show the Mn and Co exchange splittings, respectively, for Co_2MnSn as a function of their magnetic moments for different lattice constants (i.e., different applied pressure). Note the linear dependence shown by our data and the excellent agreement with experiment as far as the size of the Mn exchange splitting (about 1 eV) is concerned. Further, similar trends (not shown) are obtained for Co_2MnSi and Co_2MnGe.

In Fig. 6, we report the total (core + valence) calculated Mn and Co hyperfine fields vs applied pressure. The trend is very well reproduced by a linear fit: $H^{hf}(P)/H^{hf}(0)=1+k\cdot P$. We report in Table IV our calculated k values (with both GGA and LSDA), compared with available NMR experimental data[10] [the equilibrium values of the hyperfine fields, $H^{hf}(0)$, are given in Table III]; the hyperfine field trend is accurately reproduced, since the sign of the coefficient is always in agreement with experiment. However, while the agreement of the magnitude of k is reasonable for Mn, it is much worse for Co. The reason for this discrepancy is not clear. Note that a decomposition of the hyperfine fields into valence and core contributions reveals, as already

TABLE IV. Coefficients k (in GPa^{-1}) of the hyperfine fields vs pressure for Mn and Co for both LSDA and GGA (in units of 10^{-3}). The NMR experimental data are taken from Ref. 10.

	Co_2MnSi			Co_2MnGe			Co_2MnSn		
	LSDA	GGA	expt	LSDA	GGA	expt	LSDA	GGA	expt
k(Mn)	−1.8	−1.7	(−1.61±0.04)	−1.4	−1.5	(−1.20±0.06)	−1.6	−2.0	(−1.19±0.03)
k(Co)	−18.2	−10.1	(−4.26±0.14)	−18.9	−10.7	(−3.94±0.07)	−10.9	−8.1	(−1.82±0.07)

pointed out for the equilibrium structures, an excellent proportionality between the core Fermi contact term and the magnetic moment.[19] In contrast to what we find for Mn, we note from Figs. 6(c) and 6(d) that the total hyperfine field on the Co site increases as a function of the applied pressure, while the magnetic moment is nearly constant [or just slightly increasing, see Fig. 4(a)]. This behavior is due to the valence contribution to H^{hf}, which is more sensitive to pressure than the core contribution.

Further, recent Mössbauer experiments under pressure were performed for the Sn compound, resulting in a coefficient $[1/H^{\mathrm{hf}}_{\mathrm{Sn}}(0)]dH_{\mathrm{hf}}(P)/dP=0.022\ \mathrm{GPa}^{-1}$, to be compared to our value of 0.01 GPa^{-1}. In this case, the agreement both in sign and magnitude is reasonable. Considering that a satisfying agreement was also found for $H^{\mathrm{hf}}_{\mathrm{Sn}}(\mathrm{tot})$ at equilibrium (see Table III), we can infer that we are correctly describing the transferred hyperfine interactions for the Sn atom in this Heusler compound.

V. CONCLUSIONS

First principles FLAPW calculations were performed for Co_2MnX ($X=$Si, Ge, Sn) Heusler compounds. Our results show that the GGA is essential to recover the discrepancy between LSDA and experiments for the lattice constants and, consequently, to describe more accurately the electronic and magnetic properties of these systems. Half-metallicity is found for the Si and Ge compounds, whereas Co_2MnSn is a ''nearly'' half-metallic Heusler alloy. Their properties were discussed in terms of the X atomic substitution, applied pressure and exchange and correlation functional employed. Our calculated total magnetization is very close to 5 μ_B for all three Heusler compounds examined and is in very good agreement with recent experiments. Contact hyperfine fields were calculated and compared with experiment; a general underestimate (both at equilibrium and under pressure) was obtained for Mn, whereas reasonable agreement was found for the Co and Sn hyperfine interactions, where the GGA completely overcomes the LSDA errors. As expected,[19] the core contribution to the hyperfine field for both Mn and Co scales precisely with the local magnetic moments. Finally, the calculated Mn $2p$ exchange splitting is found to be in agreement with experiment and proportional to the Mn magnetic moments.

ACKNOWLEDGMENTS

Work at Northwestern University was supported by the U.S. National Science Foundation (through the Northwestern University Materials Research Center). We gratefully acknowledge Dr. YuJun Zhao for useful discussions and suggestions and Dr. Kohji Nakamura for assistance with the orbital moment calculations.

[1] P.R. Hammar, B.R. Bennett, M.J. Yang, and M. Johnson, Phys. Rev. Lett. **83**, 203 (1999).
[2] K.A. Kilian and R.H. Victora, J. Appl. Phys. **87**, 7064 (2000).
[3] G. Prinz, Science **282**, 1660 (1998); Y. Ohno, D.K. Young, B. Beschoten, F. Matsukura, H. Ohno, and D.D. Awschalom, Nature (London) **402**, 790 (1999); T. Dietl, H. Ohno, F. Matsukura, J. Cibert, and D. Ferrand, Science **287**, 1019 (2000).
[4] J.H. Park, E. Vescovo, H.J. Kim, C. Kwon, R. Ramesh, and T. Venkatesan, Nature (London) **392**, 794 (1998).
[5] R.A. De Groot, F.M. Mueller, P.G. Van Engen, and K.H.J. Buschow, Phys. Rev. Lett. **50**, 2024 (1983).
[6] W. Pickett, Phys. World **11**, 22 (1998).
[7] I. Galanakis, S. Ostanin, M. Alouani, H. Dreyssé, and J.M. Wills, Phys. Rev. B **61**, 4093 (2000).
[8] A. Deb, M. Itou, Y. Sakurai, N. Hiraoka, and N. Sakai, Phys. Rev. B **63**, 064409 (2001).
[9] J. Kübler, A.R. Williams, and C.B. Sommers, Phys. Rev. B **28**, 1745 (1983).
[10] M. Kawakami, Y. Kasamatsu, and H. Ido, J. Magn. Magn. Mater. **70**, 265 (1987).
[11] M. P. Raphael, S. F. Cheng, B. N. Das, B. Ravel, B. Nadgorny, G. Trotter, E. E. Carpenter, and V. G. Harris, MRS Proceedings, Spring Meeting, 2001.
[12] T. Ambrose, J.J. Krebs, and G.A. Prinz, J. Appl. Phys. **87**, 5463 (2000).
[13] S. Fujii, S. Sugimura, S. Ishida, and S. Asano, J. Phys.: Condens. Matter **2**, 8583 (1990).
[14] S. Ishida, S. Fujii, S. Kashiwagi, and S. Asano, J. Phys. Soc. Jpn. **654**, 2152 (1995).
[15] U. von Barth and L. Hedin, J. Phys. C **5**, 1629 (1972).
[16] T. Asada and K. Terakura, Phys. Rev. B **47**, 15 992 (1993); T. Asada and K. Terakura, *ibid.* **46**, 13 599 (1992).
[17] A. Continenza, S. Picozzi, W.T. Geng, and A.J. Freeman, Phys. Rev. B **64**, 085204 (2001).
[18] J.P. Perdew and Y. Wang, Phys. Rev. B **45**, 13 244 (1992); J.P. Perdew, K. Burke, and M. Ernzernhof, Phys. Rev. Lett. **77**, 3865 (1996).
[19] A. J. Freeman and R. E. Watson, in *Magnetism*, edited by G. T. Rado and H. Shul (Academic, New York, 1965), Vol. IIA; R.E. Watson and A.J. Freeman, Phys. Rev. **123**, 2027 (1961).
[20] H.J.F. Jansen and A.J. Freeman, Phys. Rev. B **30**, 561 (1984); E. Wimmer, H. Krakauer, M. Weinert, and A.J. Freeman, *ibid.* **24**, 864 (1981), and references therein.
[21] D.J. Singh, W.E. Pickett, and H. Krakauer, Phys. Rev. B **43**, 11 628 (1991).
[22] P. Mohn, P. Blaha, and K. Schwarz, J. Magn. Magn. Mater. **140-144**, 183 (1995).
[23] T. Shishidou, R. Asahi, and A.J. Freeman, Phys. Rev. B **64**, 180401 (2001).
[24] H.J. Monkhorst and J.D. Pack, Phys. Rev. B **13**, 5188 (1976).
[25] P.J. Webster, J. Phys. Chem. Solids **32**, 1221 (1971).
[26] A.G. Gavriliuk, G.N. Stepanov, and S.M. Irkaev, J. Appl. Phys. **77**, 2648 (1995).
[27] F.D. Murnaghan, Proc. Natl. Acad. Sci. U.S.A. **30**, 244 (1944).
[28] R. Fiederling, M. Klein, W. Ossau, G. Schmidt, A. Waag, and L.W. Molenkamp, Nature (London) **402**, 787 (1999).
[29] J.H. Cho and M. Scheffler, Phys. Rev. B **53**, 10 685 (1996).

[30] A.G. Gavriliuk, G.N. Stepanov, V.A. Sidorov, and S.M. Irkaev, J. Appl. Phys. **79**, 2609 (1996).

[31] Although we included spin–orbit coupling in the calculations (see below), we do not show its effect on the band structure for the sake of simplicity in the presentation.

[32] The accuracy in the position of E_F with respect to the minority VBM has been checked by increasing the number of **k** points and the k_{max} value, in order to achieve a higher level of convergence. We found that the relative alignment is stable to within 0.02 eV.

[33] Our results concerning E_{gap} and the Fermi level position with respect to the minority VBM are consistent (within 0.3 eV at most) with previous LSDA calculations (Ref. 14) with the linearized muffin-tin orbital in the atomic sphere approximation (LMTO-ASA) method (at their calculated equilibrium lattice constants). The disagreement is certainly due to the different computational methods used and specifically to their use of the ASA, which is not very accurate in the case of appreciable asphericities in the charge density (as in these Heusler compounds).

[34] It was recently argued [see K. Capelle and G. Vignale, Phys. Rev. Lett. **86**, 5546 (2001)] that spin density functional potentials are not unique functionals of the spin densities, so that our values could miss the contribution due to the discontinuity of the exchange-correlation potential, and so show a problem similar to the underestimation of the band-gap in semiconductors occurring in the original (i.e., not spin-resolved) DFT.

[35] P.J. Webster and K.R.A. Ziebeck, in *Alloys and Compounds of d-Elements with Main Group Elements, Part 2*, edited by H.R.J. Wjin, Landolt-Börnstein, New Series, Group III (Springer-Verlag, Berlin, 1988), Vol. 19, Part C, pp. 75–184.

[36] Y.M. Yarmoshenko, M.I. Katsnelson, E.I. Shreder, E.Z. Kurmaev, A. Slebarski, S. Plogmann, T. Schlatholter, J. Braun, and M. Neumann, Eur. Phys. J. B **2**, 1 (1998); S. Plogmann, T. Schlatholter, J. Braun, M. Neumann, Y.M. Yarmoshenko, M.V. Yablonskikh, E.I. Shreder, E.Z. Kurmaev, A. Wrona, and A. Slebarski, Phys. Rev. B **60**, 6428 (1999).

[37] It has been pointed out [see, M. Battocletti, H. Ebert, and H. Akai, Phys. Rev. B **53**, 9776 (1996)] that care has to be taken when dealing with the calculation of hyperfine fields within GGA; in fact, due to a divergence inherent in the general expression of the exchange potential in the GGA as the radius approaches zero, the *s* gradient density in the nuclear region could take values well beyond the range for which the GGA parametrization has been optimized. It was therefore recommended to use a ''finite nucleus model'' within GGA. In our calculations and in most recent simulations [see, for example, Ref. 8 and P. Ravindran, A. Delin, P. James, B. Johansson, J.M. Willis, R. Ahuja, and O. Eriksson, *ibid.* **59**, 15 680 (1998)] however, a ''point nucleus model'' was used, since the results for the hyperfine fields are in reasonable agreement with experiment.

[38] A.J. Freeman and R. Wu, Nuovo Cimento D **18**, 137 (1996).

[39] J.I. Lee, S.C. Hong, A.J. Freeman, and C.L. Fu, Phys. Rev. B **47**, 810 (1993).

[40] P.S. Bagus, J.V. Mallow, and A.J. Freeman, Int. J. Magn. **4**, 35 (1973); P.S. Bagus, F. Sasaki, and A.J. Freeman, Phys. Rev. Lett. **30**, 850 (1973).